Near-IR Intramolecular Charge Transfer in Strongly Interacting Diphenothiazene-TCBD and Diphenothiazene-DCNQ Push-Pull Triads

Indresh S. Yadav,^{a,‡} Youngwoo Jang,^{b,‡} Yogajivan Rout,^a Michael B. Thomas,^b Rajneesh Misra^{a,*} and Francis D'Souza^{b,*}

^aDepartment of Chemistry, Indian Institute of Technology, Indore 453552, India. E-mail: rajneeshmisra@iiti.ac.in

^bDepartment of Chemistry, University of North Texas, 1155 Union Circle, #305070, Denton, TX 76203-5017, USA, E-mail: Francis.DSouza@UNT.edu

Abstract: Three types of phenothiazines dimers (PTZ-PTZ, 1–3), covalently linked with one or two acetylene linkers, were synthesized by copper-mediated Eglinton and Pd-catalyzed Sonogashira coupling reactions in excellent yields. The dimers 1–3 were further engaged in [2+2] cycloaddition-retroelectrocyclization reactions with strong electron acceptors, tetracyanoethylene (TCNE) and 7,7,8,8-tetracyanoquinodimethane (TCNQ) to yield tetracyanobutadiene (TCBD, 1a-3a), and dicyanoquinodimethane (DCNQ, 1b-3b) functionalized donor-acceptor (D-A) conjugates, respectively. The conjugates were examined by a series of spectral, computational, and electrochemical studies. Strong intramolecular charge transfer (ICT) leading to new optical transitions was witnessed in both series of D-A conjugates. In the case of DCNQ derived D-A system 1b, the optical coverage extended until 1200 nm in benzonitrile, making this a rare class of D-A ICT system. Multiple redox processes were witnessed in these D-A systems, and the frontier orbitals generated on DFT optimized structures further supported the ICT phenomenon. Photochemical studies performed using femtosecond pump-probe studies confirmed solvent polarity dependent excited state charge transfer and separation in these novel multi-modular D-A conjugates. The charge-separated states lasted up to 70 ps in benzonitrile while in toluene slightly prolonged lifetime of up to 100 ps was witnessed. The significance of diphenothiazine in wideband optical capture all the way into the near-IR region and promoting ultrafast photoinduced charge separation in the D-A-D configured multi-modular systems, and the effect of donoracceptor distance and solvent polarity was the direct outcome of the present study.

[‡]Equal contribution

Introduction

Multi-modular π -extended donor-acceptor conjugates of the type D_n -A (where n=1,2,... etc. D= photoactive electron donor and A= electron acceptor) have attracted much attention of the scientific community due to their importance in a wide range of applications such as dyesensitized solar cells (DSSCs) and bulk heterojunction (BHJ) solar cells, $^{1-7}$ sensors, $^{8-10}$ electrochromic devices as well as optical, electronic and magnetic materials. $^{11-13}$ Synthetically, the multi-modularity could be accomplished starting from $D-\pi-\pi-D$, $D-\pi-D$, $D-\pi$ -spacer- $\pi-D$ type dimeric materials followed by introducing an electron acceptor making use of the π -spacer leading to the formation of $D-A-\pi-D$, D-A-D and D-A-spacer- $\pi-D$ type donor-acceptor conjugates. One of the advantages of this approach is placing the D and A in close proximity promoting efficient intramolecular charge transfer (ICT) both in the ground (polarization) and excited states. Although such approach has been utilized in a few studies, no systematic study on how the different types of $D-\pi-\pi-D$, $D-\pi-D$, $D-\pi$ -spacer- $\pi-D$ starting materials, and the resulting D-A-D conjugates would govern CT interactions is not known. With this goal in mind, in the present study, we have designed, synthesized, and characterized a series of multi-modular D-A-D conjugates and report their CT properties.

The photoactive electron donor chosen in the present investigation is phenothiazine (PTZ); an important class of heterocyclic compound having a tricyclic non-planar (butterfly) structure with electron-rich nitrogen and sulfur atoms, responsible for their electron-rich property. ¹⁴ The PTZs reveal reversible oxidation at low potentials due to the formation of the stable radical cation. The non-planar structure of phenothiazine (PTZ) reduces intermolecular interactions thus limiting molecular aggregation. This provides opportunities for further modification and also for tuning their optoelectronic properties, especially in D-A systems and as dyes for dye-sensitized solar cell applications. ¹⁵⁻¹⁷

Tetracyanoethylene (TCNE) and 7,7,8,8-tetracyanoquinodimethane (TCNQ) are strong electron acceptors known to undergo [2+2] cycloaddition–retroelectrocyclization reaction with electron donors carrying an acetylene group at room temperature to produce tetracyanobutadiene (TCBD) and expanded-TCBD (also known as dicyanoquinodimethane (DCNQ)) bearing D-A conjugates in good yields. Both TCBD and DCNQ are powerful electron acceptors and have the tendency to strongly interact with the electron donor revealing strong CT both in the ground and

excited states. Starting from the groundbreaking work of Diederich¹⁸ on these type of compounds, a few groups have taken advantage of this synthetic approach and reported on different types of D-TCBD and D-DCNQ derivatives, and have reported a number of fundamental discoveries on the ground and excited-state charge transfer events.¹⁹⁻³⁸

Figure 1 shows the structures of D-A- π -D, D-A-D, and D-A-spacer- π -D, D-A-spacer type conjugates derived from PTZ as an electron donor and TCBD or DCNQ as electron acceptors. Molecules **1**, **2**, and **3**, respectively, represent the D- π - π -D, D- π -D, D- π -spacer- π -D starting materials while **1a**, **2a**, and **3a** represent TCBD derived conjugates while **1b**, **2b**, and **3b** are those derived from DCNQ. Compounds **4**, **4a**, and **4b** are control compounds missing the second PTZ entity, needed to establish the role of the second PTZ in the CT process. Spectral, computational, electrochemical, and spectroelectrochemical studies were systematically performed to seek structure-property relations, and excited-state CT events have been probed by pump-probe transient spectroscopy.

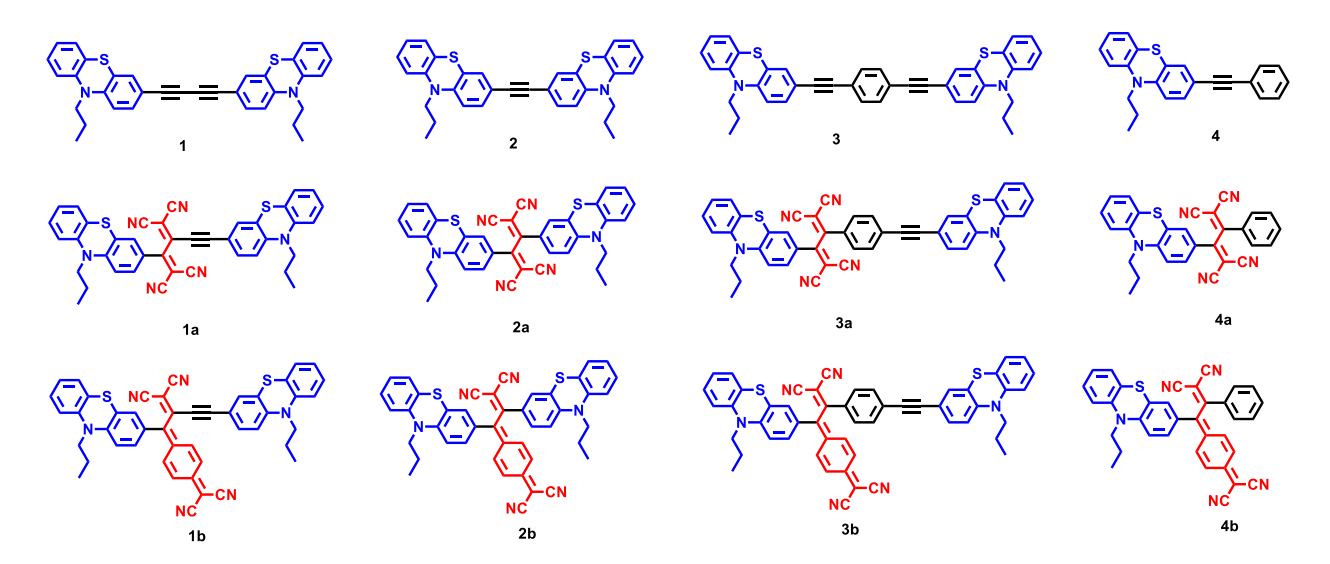


Figure 1. Structure of the investigated D-A- π -D, D-A-D, D-A-spacer- π -D and D-A (D = PTZ and A = TCBD or DCNQ) conjugates along with the phenothiazine dimers.

Results and Discussion

Synthesis

The synthetic method of phenothiazine derivatives, **1–3** is shown in Scheme 1. The copper-mediated Eglinton coupling reaction of ethynyl-PTZ (3-ethynyl-10-propyl-10*H*-phenothiazine) with use of copper acetate, MeOH, and pyridine in reflux condition for 6 h resulted in butadiynyl-

bridged diphenothiazines 1 in 75% yield.³⁹ Compounds 2 and 3 were synthesized by Pd-catalyzed Sonogashira cross-coupling reaction of PTZ-Br and commercially available 1,4-diiodobenzene with 1.2 and 2.2 equiv of ethynyl-PTZ using a catalytic amount of Pd(PPh₃)₄ added in THF:TEA (1:1) and refluxed at 60 °C for 12 h to form desire product in 62% and 65% yield, respectively.⁴⁰ Similarly, the control compound 4 was also synthesized by the reaction of iodobenzene with 1 equiv. of ethynyl-PTZ resulting in 62% yield (Scheme S3). The TCBD functionalized phenothiazine derivatives, 1a, 2a, and 3a, and control compound 4a were synthesized by [2+2] cycloaddition-retroelectrocylization reaction of 1–4 with TCNE (Scheme 2 and Scheme S1–S3). Similarly, the DCNQ functionalized phenothiazine derivatives, 1b, 2b, and 3b, and control compound 4b were synthesized by [2+2] cycloaddition-retroelectrocylization reaction of 1–4 with DCNQ in excellent yields (Scheme 2 and Scheme S1–S3). The synthetic details are given in the experimental section along with NMR and mass spectral data. The compounds were fully characterized by ¹H, and ¹³C NMR, HRMS, and Maldi-Mass techniques (See Figures S1–S36).

Scheme 1. Synthetic route of 1–3.

Scheme 2. Synthesis of 1a and 1b.

Optical properties

Figure 2a shows the absorption spectrum of 1, 1a, and 1b in benzonitrile while for all investigated compounds such spectra in benzonitrile are given in Figure S37 and the data are summarized in Table 1. Spectral patterns of PTZ dimers, 1, 2, and 3 were characterized by an intense peak in the 400 nm region that was red-shifted compared to monomeric control 4 having a peak maximum at 349 nm. That is, a bathochromic shift of over 40 nm for the dimers was witnessed as a consequence of extended π -structure and a second PTZ entity. Introducing either TCBD or DCNQ in the PTZ dimers revealed additional spectral peaks characteristic of intramolecular charge transfer (ICT or charge polarization) of the types PTZ^{δ+}-TCBD^{δ-}-PTZ and $PTZ^{\delta+}$ -DCNQ $^{\delta-}$ -PTZ. For example, in the case of 1a, the ICT band maxima were located at 564 nm while for 1b it was at 753 and 1065 nm (Figure 2a). The ICT peak extended until 850 nm in the case of 1a while for 1b it was broad covering spectral range up to 1200 nm. The spectra shown for control compounds 4a and 4b (green and magenta dashed lines in Figure 2a) brought out the importance of having PTZ dimer over a PTZ monomer, that is, extended wide-band absorption was witnessed for the PTZ dimer derived systems. The ICT peak for 4a was blue-shifted and appeared at 548 while that of 4b they were at 753 and 860 nm. That is, although ICT transitions were observed for the monomeric controls, their spectra coverage was much narrower. In addition, molar extinction of ICT peaks of 1a, and 1b were much higher than those observed for respective monomeric controls (Figure 2a). A similar trend was also observed for 2a and 2b, however, for 3a and 3b having a phenyl ring spacer between the two PTZ rings, the spectral features were close to

that of monomeric 4a and 4b (Figure S37). It appears that there are limited contributions of extended π -conjugation in 3a and 3b. The ICT transitions were also observed in nonpolar, toluene (Figure S38). However, as expected for CT transitions, the bathochromic shifts and spectral coverage of ICT peaks were relatively less in the nonpolar solvent (see Table S1).

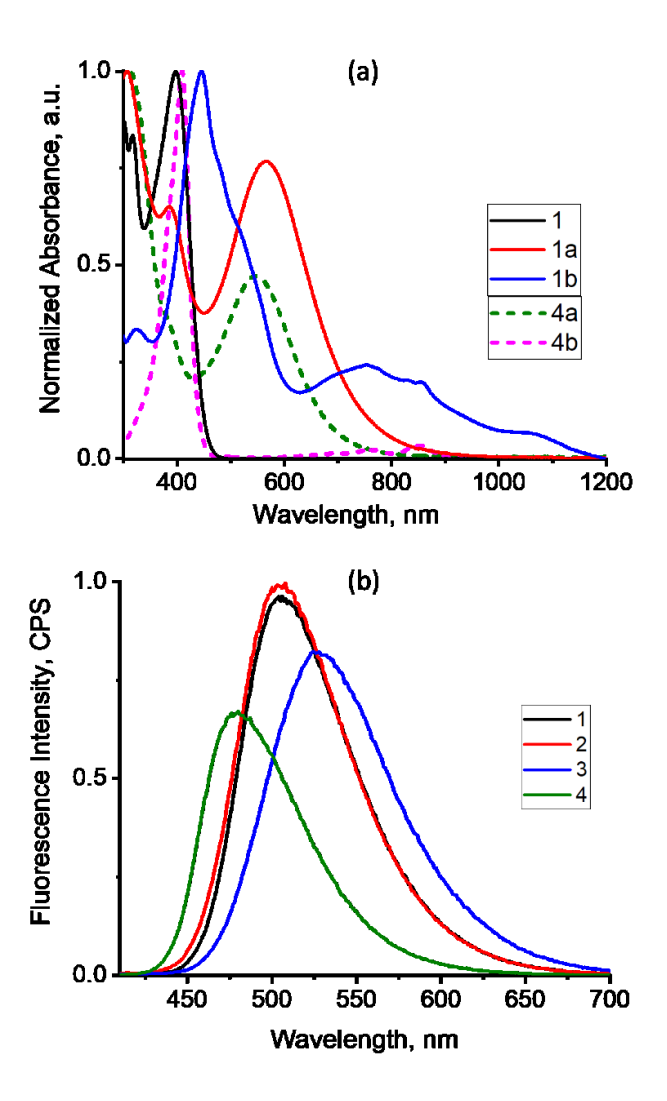


Figure 2. (a) Normalized absorption and (b) fluorescence spectra of the indicated compounds in benzonitrile. The samples were excited at their corresponding peak maxima as given in Table 1.

As shown in Figure 2b, only compounds **1–4** were found to be fluorescent. Virtually no fluorescence was detected for TCBD and DCNQ bearings systems. The emission peak maxima were red-shifted by 25–48 nm, more for **3** compared to the monomeric compound **4** (see Table 1). Fluorescence lifetimes measured using the time-correlated single-photon counting (TCSPC)

technique were found to be 2.65 ns, 2.69 ns, 2.52 ns, and 5.09 ns, respectively for **1**, **2**, **3**, and **4** (see Figure S39 for decay profiles)

Table 1. Spectral and electrochemical data from differential pulse voltammetry, and calculated energies of charge transfer, charge separation, and charge recombination for the investigated compounds in benzonitrile.

Compound		$\lambda_{\rm abs}$ (nm)			$\lambda_{\rm em}$ (nm)	$E_{0,0,}$ $\mathrm{eV^a}$	Potential V vs. Fc/Fc				E _{CT} , -	$-\Delta G_{CS}$, $-\Delta G_{CR}$, eV eV		
								E _r	ed	Ε	ox	- e v	ev	<i>E</i> v
1	301	316	398			505	2.83			0.29	0.80			
2	304	316	397			505	2.83			0.34	0.86			
3		317	391			528	2.75			0.30	0.96			
4		304	349			480	2.94			0.29	0.90			
1 a	306	385	564°					-1.12	-0.72	0.47	0.95	2.28	1.19	1.13
2a	308	385	564°					-1.13	-0.72	0.45	0.90	2.42	1.21	1.11
3a	315	377	541°					-1.56	-0.78	0.45	0.95	2.38	1.27	1.05
4a	308	383	548c					-1.23	-0.83	0.47	0.94	2.37	1.11	1.24
1b	323	445	753 ^c	1065°				-0.80	-0.33	0.37	0.70	1.77	1.15	0.82
2b	313	409	465	664 ^c	857 ^c			-0.73	-0.32	0.40	0.78	1.87	1.16	0.66
3b	408	493	680°	758 ^c	858 ^{c,d}			-0.65	-0.31	0.35	1.00	1.82	1.19	0.60
4b	408	680	753	860 ^{c,d}				-0.92	-0.32	0.38	0.91	1.79	1.18	0.64

^a-Midpoint energy of low energy absorption and fluorescence peaks

Electrochemical and spectroelectrochemical properties

Electrochemical behavior of these push-pull systems was subsequently performed using both cyclic (CV, to verify reversibility) and differential pulse (DPV, to determine the peak potentials) in *o*-dichlorobenzene (DCB) containing 0.1 M (TBA)ClO₄. Figure 3 illustrates representative DPVs, while complete CVs and DPVs for the entire series of compounds are given in Figures S40–S43 in SI. Compounds **1–4** having one or two PTZs revealed no reduction within

^b-gas phase HOMO-LUMO gap from DFT studies

^c-polarized CT transition

^d- weak molar absorptivity

the accessible potential window, however, two oxidation processes during the anodic scan of the potential were witnessed. The first oxidation process was located in the 0.29–0.34 V vs. Fc/Fc⁺ potential range (see Table 1). Incorporation of electron-deficient TCBD or DCNQ revealed two-one-electron reductions corresponding to TCBD^{0/.-} and TCBD^{-/2-} processes in the case of **1a**, **2a**, **3a**, and **4a** and DCNQ^{0/.-} and DCNQ^{-/2-} processes in the case of **1b**, **2b**, **3b** and **4b**. The TCBD^{0/.-} process appeared in the -0.72 to -0.83 V range while DCNQ^{0/.-} process appeared in the -0.31 to -0.33 V range. That is, a facile reduction of DCNQ over TCBD was witnessed. Having electron-deficient TCBD or DCNQ also affected the oxidation potentials of PTZ due to electronic induced effects. In the case of **1a**, **2a**, **3a**, and **4a**, the first oxidation process was difficult by ~150 mV while for **1b**, **2b**, **3b**, and **4b** such effect was relatively less, being ~50 mV although DCNQ was a better electron acceptor. This has been rationalized to the extended π -structure of DCNQ lessening the inductive effects. The electrochemical gap (potential difference between the first oxidation and

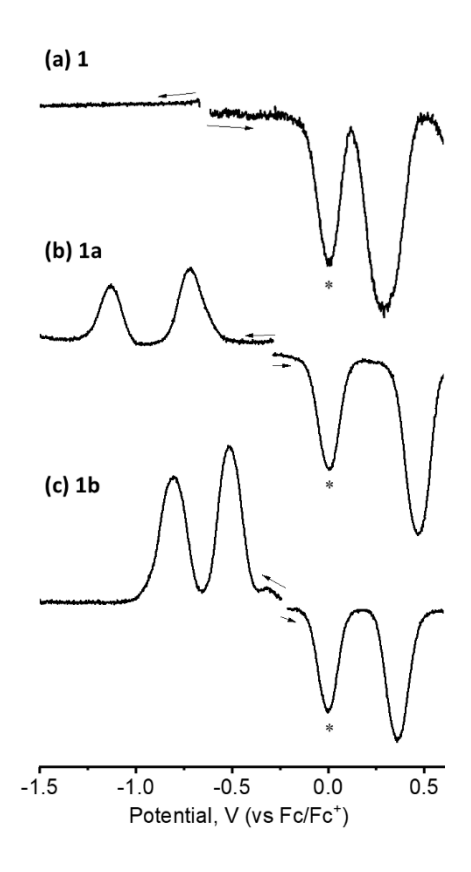


Figure 3. DPVs of the indicated push-pull systems in *o*-dichlorobenzene containing 0.1 M (TBA)ClO₄. The asterisk shows the oxidation of ferrocene used as an internal standard.

first reduction processes) was found to range between 1.17 to 1.30 V in the case of 1a-4a series that compared with values of 0.66 to 0.88 V in the case of 1b-4b series of compounds (abbreviated as $E_{\rm CT}$ in Table 1). The red-shifted charge transfer bands for the 1b-4b series of compounds could be attributed to the smaller gaps.

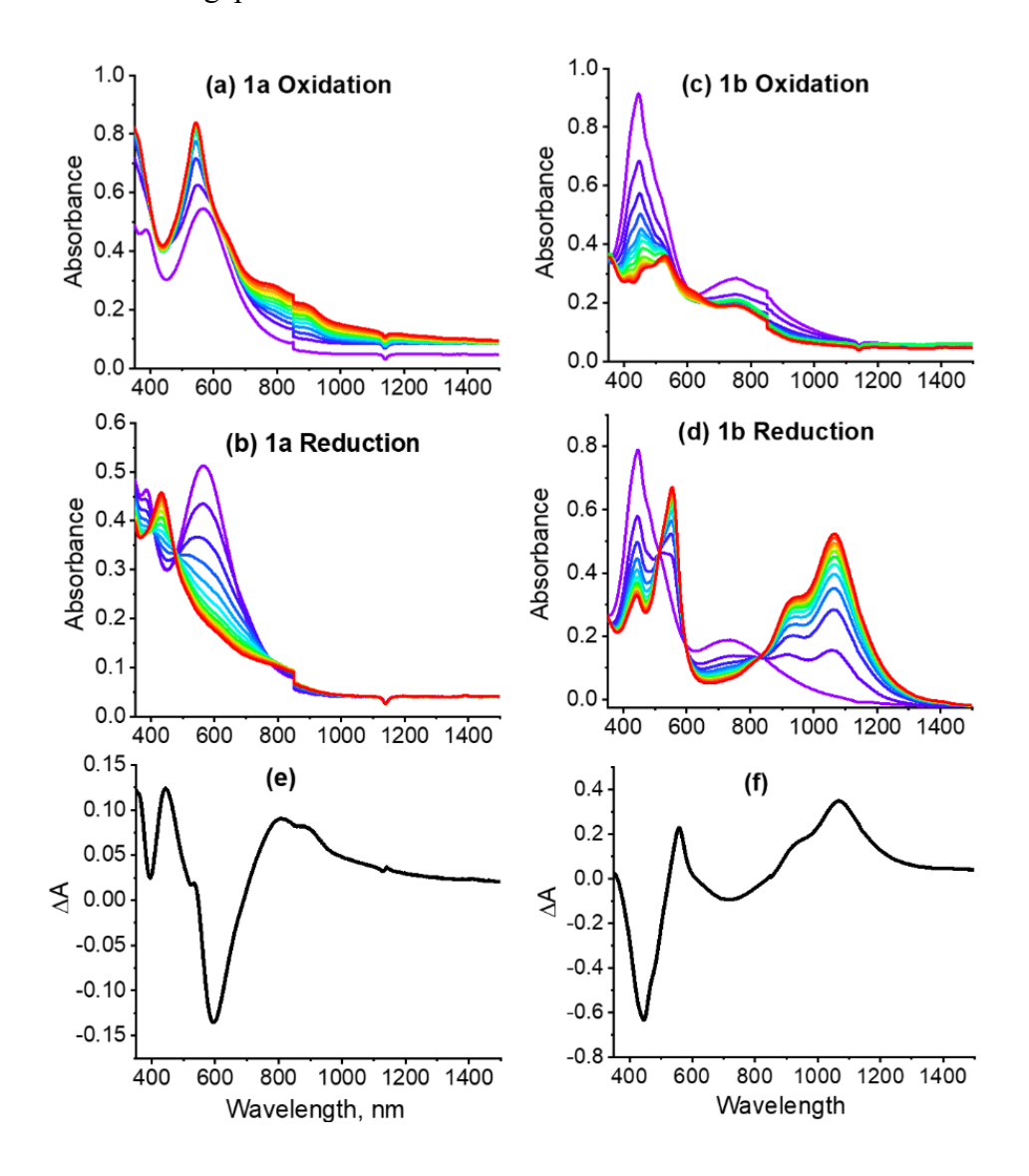


Figure 4. Spectral changes during first oxidation and first reduction of 1a and 1b in benzonitrile containing 0.2 M (TBA)ClO₄. The bottom panel shows the spectrum deduced for the charge-separated product of 1a and 1b (see text for details).

Spectroelectrochemical studies were subsequently performed for the investigated series of compounds during their first oxidation and first reduction processes. Figure 4 shows spectral changes observed during first oxidation and first reduction of **1a** and **1b** while for other compounds

such spectral data are shown in Figures S44–S46 while Table S2 lists peak maxima of radical cationic and radical anionic species. To summarize, the one-electron oxidized product of compounds 1–4 revealed new absorption peaks covering the visible and near-IR regions. Having TCBD in 1a–4a or DCNQ in 1b–4b dampened the intensity of these cationic peaks, however, such peaks were still present. One-electron reduction of TCBD in 1a–4a revealed a reduction of peak intensities corresponding to the charge transfer bands with the appearance of new peaks in the visible region, in some instances as a shoulder band. Interestingly, the one-electron reduction of DCNQ in 1b–4b was better defined and revealed new peaks in the near-IR region covering 800-1400 nm. By digitally adding the final spectrum of the cation and anion species, and subtracting it from the neutral compound, the spectrum corresponding to the charge separation (electron transfer) product was arrived, as shown in Figure 4 bottom panel. Such spectra would be helpful in characterizing the charge separation products generated by photoexcitation in pump-probe spectroscopy (vide infra).

Electronic structure and energy level diagram

In order to visualize the push-pull effects and the overall geometry, the structures were optimized at the B3LYP/6-31G* basis set, and functional, 41 and frontier orbitals were generated. Figure 5 shows optimized structures and frontier HOMO and LUMO of 1, 1a, and 1b while results on remaining compounds along with orbital energies are given in Figures S47–S50. In all the optimized structures, no steric hindrance between PTZ and TCBD or DCNQ was noticed. For compounds 1–4, the majority of the HOMOs were on PTZ entities with appreciable contributions on the bridging acetylene linkers. Much of the LUMO was on the acetylene bridge while LUMO+1 was on the PTZ entities. Interestingly, in the case of 1a, the HOMO was on the PTZ entity which was close to TCBD while for 2a and 3a, it was on the PTZ entity that was away from TCBD. As expected, the LUMO was on TCBD with some contributions on the PTZ entities. This trend was also observed for compounds 1b–3b. In the case of 1b the HOMO was on the PTZ entity close to DCNQ, while for 2b and 3b, it was on PTZ entity away from DCNQ. In all the cases, the majority of LUMO was on the DCNQ entity. The switching of HOMO location in 1a and 1b compared to that in 2a, 3a, 2b, and 3b was witnessed from this study. As shown in Figures S48–S49, in the case of 1b and 2b, charge transfer from HOMO-1 to LUMO level is also a plausibility. Under

such circumstances, the E_{CT} value would be relatively much higher than that are shown in Table 1.

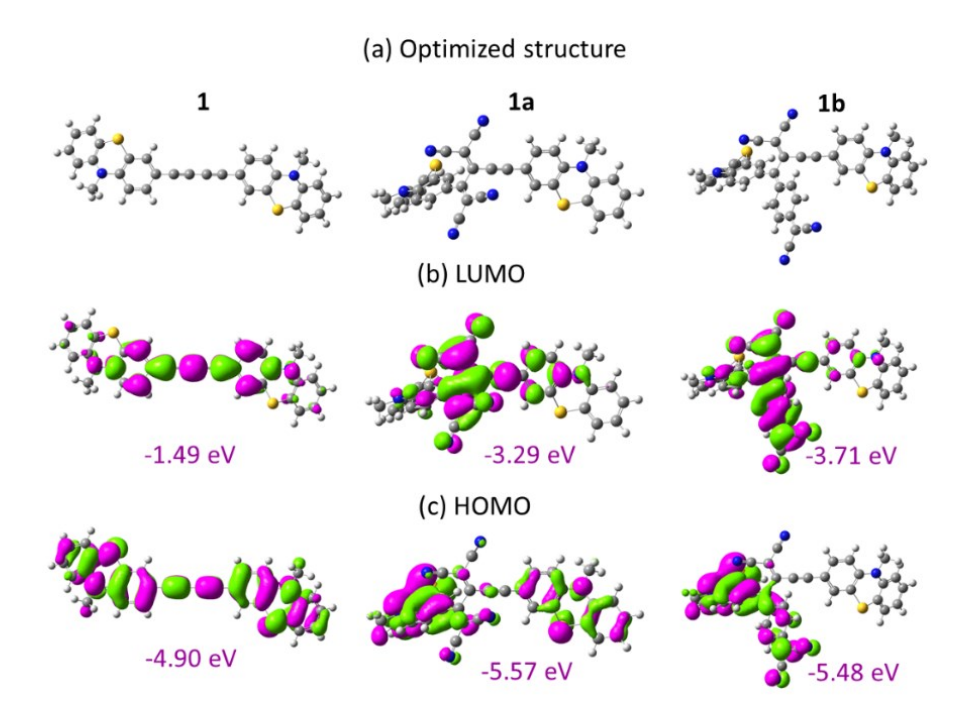


Figure 5. B3LYP/6-31G* optimized structures and frontier HOMO and LUMO of 1, 1a, and 1b.

An energy diagram was subsequently established to help in probing the excited-state charge transfer and separation events in the TCBD and DCNQ bearing push-pull systems according to Rehm-Weller's approach, ^{42,43} and is shown in Figure 6. The singlet and triplet energies were derived from absorption/fluorescence mid-point energy and phosphorescence peak maxima (see Figure S58 for phosphorescence spectrum of selected compounds). Briefly, direct excitation of PTZ at its locally excited (LE) peak maxima would populate the ¹PTZ* state, and based on earlier discussed spectral and computational results, this would involve producing the charge transfer state, PTZ⁸⁺-A⁸⁻-PTZ (A = TCBD or DCNQ) involving one of the PTZ entities (PTZ closely positioned to TCBD and DCNQ in the case of 1a and 1b, and PTZ distantly positioned in the case of 2a, 3a, 2b and 3b as predicted by the frontier orbitals) or populating the triplet excited state via the process of intersystem crossing. In the case of TCBD derived push-pull systems (1a-4a), the triplet state energies are close to the CT state. If the CT state dominates then one could expect energetically feasible, subsequent charge separation, especially in polar benzonitrile. In the case of DCNQ derived systems (1b-4b), CT state energies are lower than that

of the triplet excited state, suggesting CT to be the likely process. As shown in the energy diagram, in both benzonitrile and toluene charge-separated state is possible, although in toluene the driving force for conversion of CT to CS state is smaller. In all of the push-pull systems, as no fluorescence from PTZ was observed, the majority of the ${}^{1}PTZ^{*}$ could be expected to follow the charge transfer path yielding dipolar $PTZ^{\delta+}$ - $A^{\delta-}$ -PTZ (in the case of **1a**, **1b**, **3a**, **3b**, **4a** and **4b**) or quadrupolar $PTZ^{\delta+}$ - $A^{\delta-}$ - $PTZ^{\delta+}$ (in the case of **2a** and **2b**, due to proximity of both PTZ entities to the central TCBD or DCNQ). The charge transfer state could also be generated by direct excitation of the low-energy polarized charge transfer band. The singlet excited ${}^{1}(PTZ^{\delta+}$ - $A^{\delta-}$ - $PTZ)^{*}$ or ${}^{1}(PTZ^{\delta+}$ - $A^{\delta-}$ - $PTZ^{\delta+}$)*

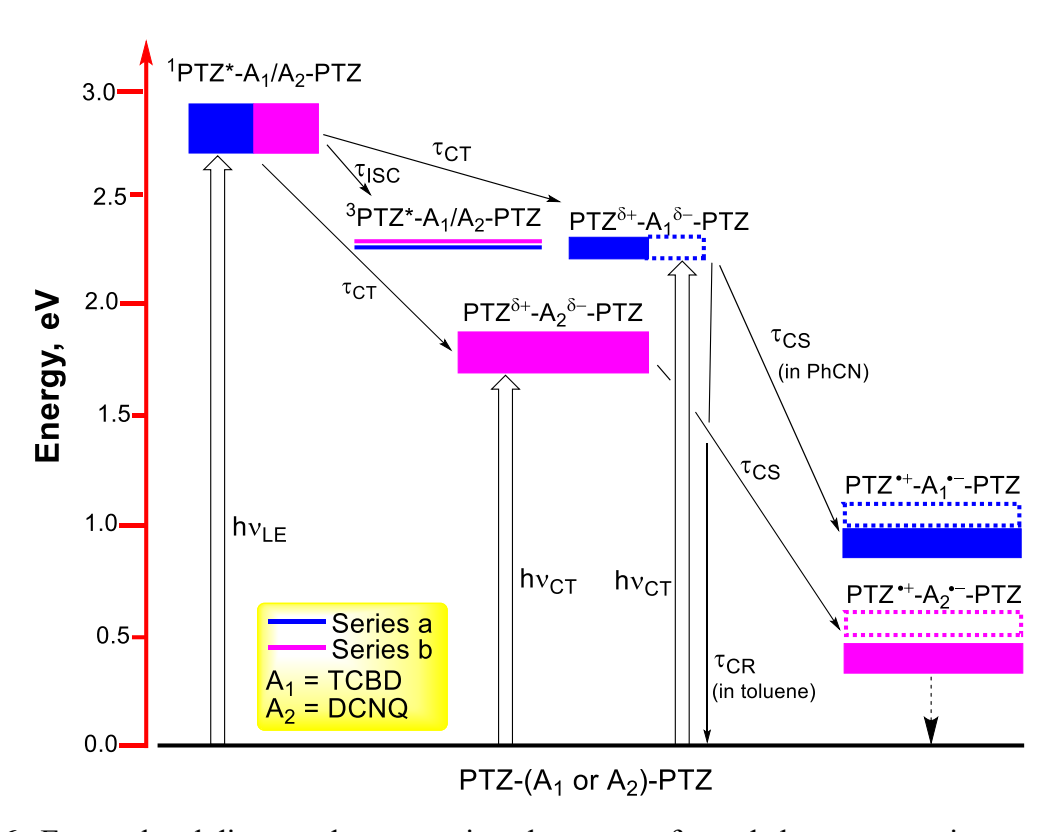


Figure 6. Energy level diagram demonstrating charge transfer and charge separation events upon photoexcitation of the phenothiazine entity, as a function of solvent polarity, in the studied pushpull systems. The height and location of the rectangles represent the energy range among the systems studied for a given photo event. The energy of the charge transfer states, $PTZ^{\delta+}$ - $A_1/A_2^{\delta-}$ -PTZ is the energy difference between HOMO and LUMO levels arrived from the DFT calculations. Under the conditions of λ_{CT} excitation, the excited state species is the excited singlet charge transfer complex, ${}^{1}(PTZ^{\delta+}$ - $A_1/A_2^{\delta-}$ -PTZ)*; not shown in the diagram for brevity. The energy of the charge-separated states was calculated from the Rehm-Weller approach in benzonitrile (solid rectangle) and in toluene (dotted rectangle).

states produced by this mechanism could undergo a subsequent charge-separated state, more so in polar benzonitrile, as shown in the energy diagram. Femtosecond pump-probe spectroscopic studies were subsequently performed to secure evidence for such mechanistic details and the data were subjected to global target analysis to seek kinetic values of different events.

Femtosecond transient absorption (fs-TA) studies

Figure S51 in SI shows the fs-TA spectra of compounds 1–4 in benzonitrile excited at 395 nm. The PTZ dimers, 1-3, and that of monomer, 4, transient spectral features were straightforward. Upon photoexcitation, all of them revealed a negative peak in the 475–550 nm range, and by compassion with their respective fluorescence peak maxima, this was attributed to stimulated emission (SE). In addition, an excited state absorption (ESA) peak in the 450 nm region was observed. Slow recovery of the SE peak and decay of the ESA peak was accompanied by a new peak in the 600–700 nm range started developing, and was attributed to ³PTZ* formed via the process of intersystem crossing.

Next, compounds **4a** and **4b** having a single PTZ entity and either TCBD or DCNQ electron acceptor were investigated for their relative structural simplicity. Figure 7a(i) and 7b(i), respectively, show fs-TA at the indicated delay times of **4a** and **4b** in benzonitrile. At the excitation wavelength of 567 nm, the CT state is mainly excited in the case of **4a**. Photochemical events were rather too fast, that is, the instantaneously formed ¹CT* revealed ultrafast transformation. In the case of **4a**, the spectrum shown at 2.17 ps revealed ESA at 486 and 742 nm and a ground state bleach (GSB) at 550 nm. The ESA could be attributed to transitions involving higher CT states. Decay and recovery of ESA and GSB peaks developed a new spectrum with a peak in the 700 nm range largely resembled the spectrum deduced for the charge-separated state from the earlier discussed spectroelectrochemical studies (see the dashed magenta line in Figure 7a(ii)). The data were subjected to Glotaran target analysis⁴⁴ with two components fit representing ¹CT* → CS. Species associated spectra (SAS) and the population time profiles are shown in Figures 7a(ii) and (iii), respectively. It may be mentioned here that the spectrum corresponding to the charge transfer and charge-separated states resemble closer, in the later state, some spectral shifts due to solvation could be expected.

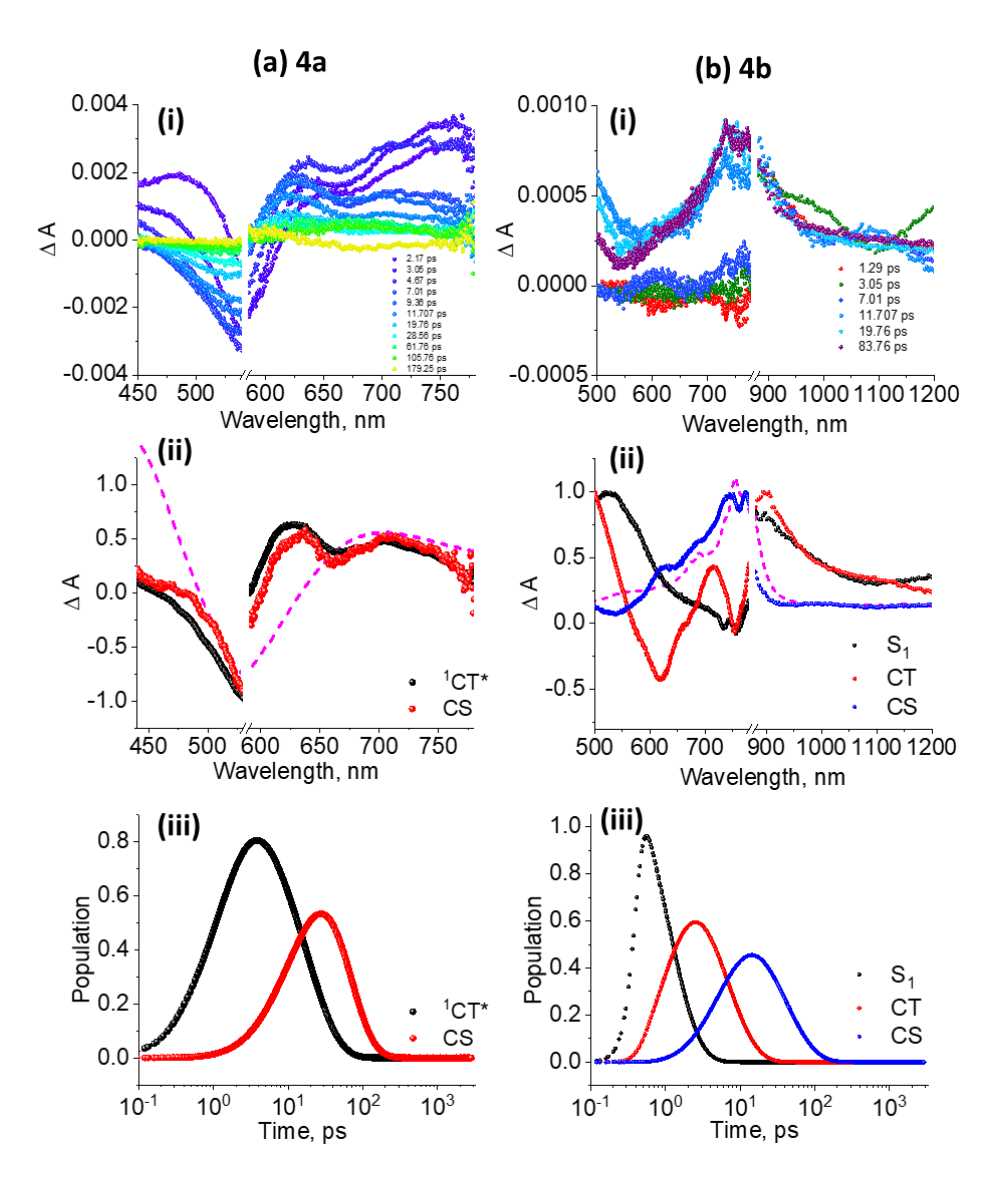


Figure 7. Fs-TA spectra at the indicated delay times of (a) 4a and (b) 4b in benzonitrile ($\lambda_{ex} = 567$ nm and 480 nm, respectively). Species associated spectra and population kinetics from Glotaran analysis are shown beneath. The dashed line in the central panel corresponds to the spectrum deduced from spectroelectrochemical studies.

Ultrafast photo-events were also witnessed in the case of **4b**, as shown in Figure 7b(i). In this case, at the excitation wavelength of 480 nm mainly LE peak instead of polarized CT peak occurs. GSB in the 750 nm range and ESA in the 520 nm range were initially witnessed (see spectrum at 1.20 ps). This species transformed into another intermediate species (see spectrum at 3.06 ps) with a depleted peak in 620 and a positive peak in the 860 nm region, attributable to an intermediate charge transfer state. The intermediate state transformed into a final state with a broad peak in the 800–900 nm range, expected for the charge-separated state from the earlier discussed

spectroelectrochemical studies (see dashed line in Figure 7b(ii)). SAS generated from Glotaran analysis with three components fit (stepwise ${}^{1}S_{1}^{*} \rightarrow CT \rightarrow CS$) and population kinetics are shown in Figure 7b(ii) and 7b(iii), respectively. Time constants evaluated through this method are given in Table 2. Important to note here is the close spectral resemblance of the spectrum corresponding to the CS state and that from the spectroelectrochemical studies, providing evidence of charge separation.

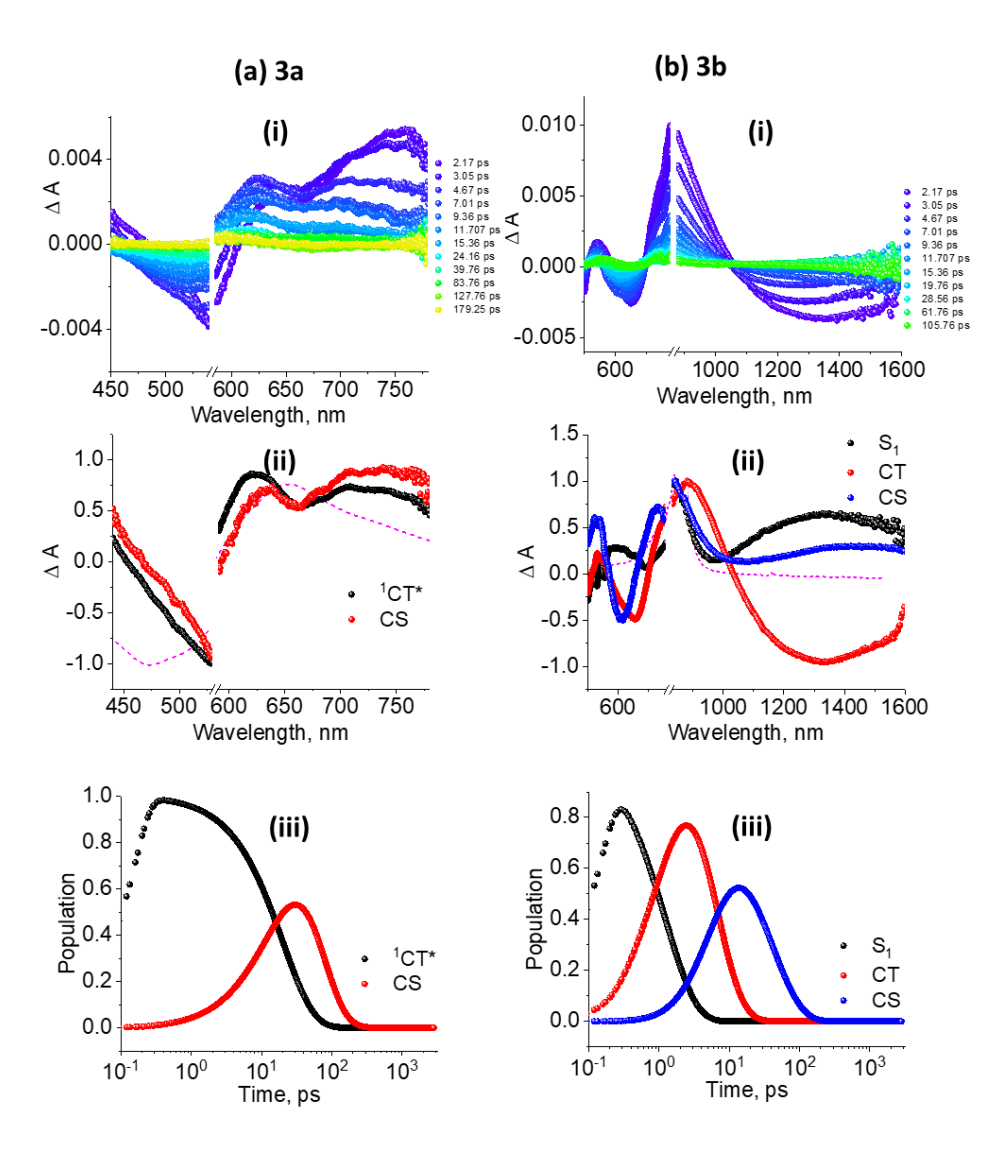


Figure 8. Fs-TA spectra at the indicated delay times of (a) **3a** and (b) **3b** in benzonitrile. **3a** was excited at 567 nm corresponding to the charge transfer state while **3b** was excited at 480 nm corresponding to the locally excited state. Species associated spectra and population kinetics from Glotaran analysis are shown beneath. The dashed line in the central panel (ii) corresponds to the spectrum deduced from spectroelectrochemical studies.

Next, TCBD or DCNQ bridged PTZ-dimers were investigated. Figure 8 shows fs-TA spectral data on 3a and 3b while those of 1a, 1b, 2a, and 2b are shown in Figures S52 and S53. In the case of 3a, the instantaneously formed excited charge-transfer species revealed the main ESA peak at 758 nm and GSB at 540 nm (see spectrum at 2.17 ps). With time, this peak revealed a redshift with an additional peak with maxima at 702 nm. Results of Glotaran analysis are shown in Figure 8a(ii) and (iii) for the sequential ${}^{1}\text{CT}^{*} \rightarrow \text{CS}$ process. In the case of 3b, as shown in Figure 8b, the formation of intermediate CT and then CS from S_{1} was obvious. In this case, the Glotaran analysis was much helpful to visualize the conversion of S_{1} to CT state, followed by CT conversion to the CS state. There was a better match of spectroelectrochemically deduced charge-separated state spectrum to the experimentally obtained one.

Table 2. Time constants for charge transfer and separation from Glotaran analysis of the transient spectral data as a function of solvent polarity.

Compound	λ _{ex} , nm	Solvent	τ _{s1} , ps	τ _{cτ} , ps	τ _{cs} , ps	τ _{T1} , ns
	ex′	Joivent	S1′ '	CT' '	cs' '	T1′
1 a	567	PhCN		16.14	37.64	
		Toluene		20.09		80.07
2a	567	PhCN		17.25	40.83	
		Toluene		20.22		87.04
3 a	567	PhCN		20.16	47.66	
		Toluene		24.04	109.92	
4 a	567	PhCN		17.25	41.29	
		Toluene		22.73	91.12	
1b	480	PhCN	< 1	7.50	28.64	
		Toluene	3.93	16.37	41.98	
2b	480	PhCN	< 1	5.65	36.22	
		Toluene	4.17	26.13	45.87	
3b	480	PhCN	< 1	5.27	38.75	
		Toluene	1.25	17.30	67.52	
4b	400	PhCN	<1	4.49	36.88	
		Toluene	4.37	11.90	52.91	

Similar transient spectral features were also observed for other systems, as shown in Figures S52 and S53. A two-step, sequential occurrence of ${}^{1}CT^{*} \rightarrow CS$ in the cases of 1a and 2a, and a three-step $S_{1} \rightarrow CT \rightarrow CS$ in the case of 1b and 2b, from Glotaran was satisfactory to explain the photo events. Importantly, such analysis helped in establishing the occurrence of charge separation in polar benzonitrile. Time constants for different photo events from Glotaran analysis is summarized in Table 2.

The earlier discussed spectral and energy diagram also predicted charge transfer and charge separation in nonpolar toluene (Figure 6), however, in the cases of **1a-4a** (push-pull systems derived from TCBD), the energy of the CT states ($E_{\text{CT}} \sim 2.28\text{-}2.42 \text{ eV}$) were close to the triplet energy states ($E_{\text{T}} \sim 2.28\text{-}2.32 \text{ eV}$). Under such conditions, the formation of charge transfer would compete with the population of the triplet state or a ping-pong effect between these two states. The CT state eventually could result in a charge-separated state. In the case of **1b-4b** (push-pull systems derived from DCNQ), however, the E_{T} is higher than that of E_{CT} , suggesting CT followed by CS is the preferred path. Consequently, transient spectral studies were also performed in toluene. Figure S54 shows the fs-TA spectra at the indicated delay times of PTZ derived compounds **1–4**. In the monitoring spectral window, broad ESA with peak maxima in 600–700 nm and 775 nm range was witnessed, however, for monomeric **4**, the ESA peak was blue-shifted and appeared in the 550–600 nm range. Decay of the ESA peak started developing a new peak with maxima in the 550-600 nm range (for **4** in the 550 nm range) attributable to the formation of 3 PTZ*.

Fs-TA spectra of 1a and 1b in toluene is shown in Figure 9a and b, respectively. In the case of 1a at the CT excitation wavelength, the spectrum recorded at the earliest delay time of 2.17 ps, revealed ESA peaks in the 450 nm region and another major peak at 704 nm accompanied by a shoulder peak at 725 nm. A GSB in the 550 nm was also witnessed. Rapid decay and recovery of these peaks resulted in a new short-lived peak in the 600 nm region. A two-component fit was satisfactory in Glotaran analysis whose SAS spectra are depicted in Figure 9a(ii). As mentioned earlier, if the CT state is transformed into a CS state, then one would expect their spectra to resemble close to each other. However, the spectrum matched largely that expected for the triplet excited state with peak maxima in the 600 nm region. These results suggest the 1 CT* \rightarrow T path for 1a in toluene.

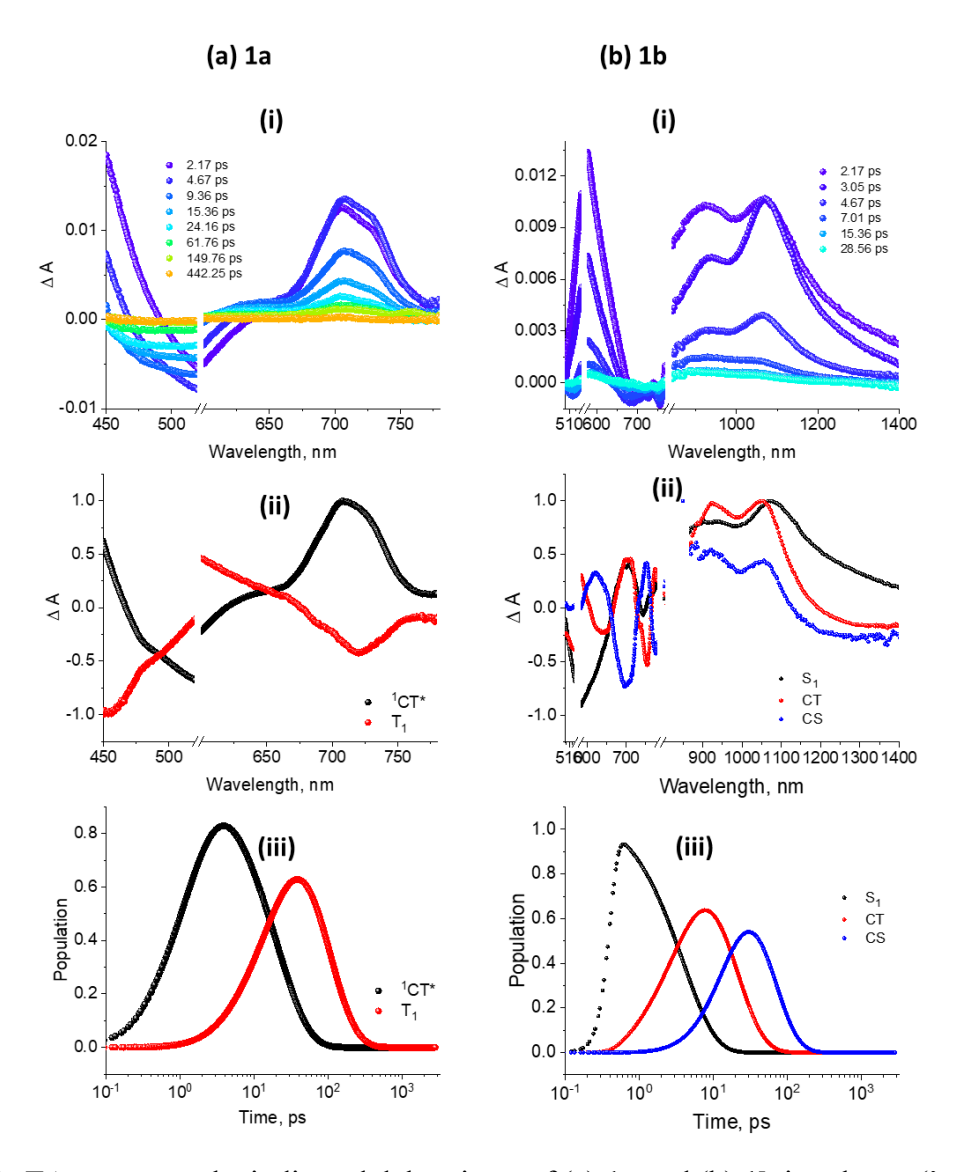


Figure 9. Fs-TA spectra at the indicated delay times of (a) **1a** and (b) **1b** in toluene ($\lambda_{ex} = 567$ nm and 480 nm, respectively). Species associated spectra and population kinetics from Glotaran analysis are shown beneath.

On the contrary, in the case of **1b**, the spectrum recorded by LE excitation at a delay time of 2.17 ps revealed ESA peaks in the 558, 920, and 1067 nm. Within the next few ps, the spectrum transformed into a new, close resembling features with the previous spectrum with peak maxima at 570, 934, and 1065 nm. The final spectrum was more or less what was predicted for the charge-separated state for this compound in Figure 4f suggesting the occurrence of charge separation in toluene. The SAS spectra generated from Glotaran analysis were supportive of $S_1 \rightarrow CT \rightarrow CS$ sequence, as shown in Figure 9b(ii). These results clearly show charge separation in **1b** but not in the case of **1a** in toluene.

As shown in Figure S55 in SI for compounds 2a and 2b, the transient spectral trends and global analysis results were similar to that observed for 1a and 1b in toluene. That is, the ${}^{1}CT^{*} \rightarrow T$ path for 2a and $S_{1} \rightarrow CT \rightarrow CS$ sequence for 2b was obvious. Time constants for different events from population time profiles are given in Table 2.

Results obtained for **3b** and **4b** in toluene were also followed by the trend of $S_1 \rightarrow CT \rightarrow CS$ sequence as shown in Figures S56(b) and S57(b). However, as shown in Figures S56(a) and S57(a), for **3a** and **3b**, the spectral features supportive of ${}^{1}CT^* \rightarrow T$ transformation wherein the final spectrum matched that expected for the triplet state. Time constants for different photo events for population kinetics are also given in Table 2.

The time constants representing the average lifetime of a given species, as a function of the structure of the push-pull systems and solvent polarity as listed in Table 2 reveal the following. First, due to high exergonicity and the close proximity of the donor and acceptor entities of the push-pull systems, the photo events are rather fast. In benzonitrile, the charge transfer events occur within 4-7 ps for **1b-4b** while this process is relatively slow and occurs in 16-22 ps in the case of **1a-4a**. In toluene, as expected for a nonpolar solvent, the CT occurs relatively slow (10-22 ps) in both TCBD and DCNQ carrying push-pull systems. In benzonitrile, the charge-separated state persists for about 37-110 ps for **1a-4a** while these values are 36-42 ps for **1b-4b**. The CS states in toluene in the case of **1b-4b** were a little long-lived with values of 42-67 ps. Among the different systems, better charge stabilization was witnessed in the case of **3a** and **3b** which could be attributed to relatively large donor-acceptor distances (see Figure S49). The significance of the nature of electron-accepting TCBD or DCNQ groups and its placement with the PTZ-dimer structure and solvent polarity in governing photochemical events and the lifetime of the charge-separated states is borne out from this study.

Summary

The newly synthesized multi-modular push-pull systems derived from phenothiazine dimers carrying either TCBD or DCNQ revealed several interesting properties. Noteworthy observations include: (i) the success of the Pd-catalyzed Sonogashira cross-coupling reaction followed by [2+2] cycloaddition-retroelectrocyclization reaction with strong electron acceptors, to yield both TCBD and DCNQ containing push-pull systems on dimeric phenothiazine skeleton; (ii) owing to the facile reduction of DCNQ over TCBD, presence of strong ground state charge transfer

(charge polarization) in the former systems extending the absorption well into the near-IR region; (iii) prediction of charge transfer and separation in polar and nonpolar solvents; (iv) combining spectroelectrochemical results with species associated spectra from Glotaran analysis of femtosecond transient data to secure evidence of charge separation; and (v) witnessing ultrafast charge transfer in these novel push-pull systems benzonitrile and toluene in few instances. The importance of multi-modular intramolecular charge-transfer complexes of the type D-A-D extending the optical coverage into the near-IR region while also exhibiting solvent and donor-acceptor distance-dependent, ultrafast charge transfer/separation upon photoexcitation are borne out from this investigation.

Experimental Section

General methods

All the chemicals were used as received unless otherwise indicated. All oxygen or moisture-sensitive reactions were performed under nitrogen/argon atmosphere using the standard schlenk method. All the chemicals were purchased from commercial sources and used without further purification. 1 H NMR (400 MHz), and 13 C NMR (100MHz) spectra were recorded on the Bruker Avance (III) 400 MHz, using CDCl₃ as a solvent and the chemical shifts were reported in parts per million (ppm) with TMS (0 ppm) and CDCl₃ (77.00) as standards. Tetramethylsilane (TMS) was used as reference for recording 1 H (of residual proton; $\delta = 7.26$ ppm), and 13 C ($\delta = 7.26$ ppm) spectra in CDCl₃. HRMS was recorded on Brucker-Daltonics, micrO TOF-Q II mass spectrometer.

The UV-visible spectral measurements were carried out with a JASCO-670 UV-visible-near IR spectrophotometer. The fluorescence emission was monitored by using a Horiba Yvon Nanolog coupled with time-correlated single-photon counting with nanoLED excitation sources. A right-angle detection method was used. Differential pulse and cyclic voltammograms were recorded on an EG&G 263A electrochemical analyzer using a three-electrode system. A platinum button electrode was used as the working electrode. A platinum wire served as the counter electrode and an Ag/AgCl electrode was used as the reference electrode. Ferrocene/ferrocenium redox couple was used as an internal standard. All the solutions were purged prior to electrochemical and spectral measurements using argon gas. Thin-layer spectroelectrochemical

measurements were performed using SEC-C thin-layer spectroelectrochemical kit from CH Instruments, Inc., Austin, TX.

Femtosecond transient absorption spectroscopy experiments were performed using an ultrafast femtosecond laser source (Libra) by Coherent incorporating a diode-pumped, mode-locked Ti:sapphire laser (Vitesse) and a diode-pumped intracavity doubled Nd:YLF laser (Evolution) to generate a compressed laser output of 1.45 W. For optical detection, a Helios transient absorption spectrometer coupled with a femtosecond harmonics generator, both provided by Ultrafast Systems LLC, was used. The sources for the pump and probe pulses were derived from the fundamental output of Libra (Compressed output 1.45 W, pulse width 100 fs) at a repetition rate of 1 kHz; 95% of the fundamental output of the laser was introduced into a TOPAS-Prime-OPA system with a 290–2600 nm tuning range from Altos Photonics Inc., (Bozeman, MT), while the rest of the output was used for generation of a white light continuum. Kinetic traces at appropriate wavelengths were assembled from the time-resolved spectral data. Data analysis was performed using Surface Xplorer software supplied by Ultrafast Systems. All measurements were conducted in degassed solutions at 298 K. The estimated error in the reported rate constants is $\pm 10\%$.

Synthetic procedure of Compound 1-4

Compound 1: In 100 mL round bottomed flask ethynyl-PTZ (500 mg ,1.88 mmol) was dissolved in MeOH (5 mL) and added as solution (513 mg, 2.82 mmol) of copper (II) acetate monohydrate in mixture of MeOH (3 mL) and pyridine (8 mL). This reaction mixture was reflux for 6 h. Upon completion of reaction, the mix. was evaporated to dryness under reduced pressure, and the crude was purified by column chromatography by using SiO₂ with Hexane/DCM (3:2, v/v) (eluent: CH₂Cl₂) to yield **PTZ 1** as yellow solid (yield: 750mg, 75%). ¹**H NMR (400 MHz, CDCl₃):** δ 7.29-7.27 (m, 2H), 7.24 (s, 2H), 7.16-7.09 (m, 4H), 6.92 (t, J = 8.0 Hz, 2H), 6.84 (d, J = 8.0 Hz, 2H), 6.75 (d, J = 8.0 Hz, 2H), 3.80 (t, J = 8 Hz, 4H), 1.86-1.77 (m, 4H), 1.00 (t, J = 4Hz, 6Hz); ¹³**C NMR (100 MHz, CDCl₃):** δ 145.77, 144.01, 131.49, 130.52, 127.15, 127.03, 124.47, 123.67, 122.57, 115.27, 115.05, 114.69, 80.99, 73.70, 48.99, 19.72, 10.92 ppm; **HRMS (ESI, positive):** m/z [M]⁺ calculated for C34H28N2S2 528.1694, found 528.1688.

Compound 2: In 100 mL round bottomed flask, PTZ-Br (500 mg, 1.5 mmol) and ethynyl-PTZ (498 mg, 1.8 mmol) were dissolved in THF: Triethylamine (10: 3, v/v; 50 mL), and reaction

mixture was purged with argon, and Pd(PPh₃)₄ (90 mg, 0.05mmol), and CuI (14 mg, 0.05 mmol) were added. The reaction mixture was stirred at 80 °C for overnight. Upon the completion of the reaction, the solvent was evaporated and purified by silica gel column chromatography with hexane/DCM (4:1, v/v) to get the desired **PTZ 2** as a yellow solid. (Yield: 490 mg, 62%). ¹H **NMR (400 MHz, CDCl₃):** δ 7.24 (s, 4H), 7.16-7.10 (m, 4H), 6.91 (t, J = 8 Hz, 2H), 6.84 (d, J = 8 Hz, 2H), 6.77 (d, J = 8Hz, 2H), 3.81 (t, J = 8 Hz, 4H), 1.76-1.87 (m, 4H), 1.01 (t, J = 4 Hz, 6H); ¹³C **NMR (100 MHz, CDCl₃):** δ 145.04, 144.63, 130.53, 129.96, 127.41, 127.24, 124.72, 124.19, 122.61, 117.14, 115.46, 114.99, 88.59, 49.22, 20.04, 11.25 ppm; **HRMS (ESI, positive):** m/z [M]⁺ calculated for C32H28N2S2 504.1694, found 504.1688.

Compound 3: In 100mL round bottomed flask, 1,4-diiodobenzene (200 mg, 0.60 mmol) and ethynyl-PTZ (353 mg, 1.3 mmol) were dissolved in THF: Triethylamine (4:1, v/v; 50 mL), and reaction mixture was purged with argon, and Pd(PPh₃)₄ (35 mg, 0.03 mmol), and CuI (5.7 mg, 0.03 mmol) were added. The reaction mixture was stirred at 60 °C for 12 h. Upon the completion of the reaction, the solvent was evaporated and purified by silica gel column chromatography with hexane/DCM (4:1) to get the desired **PTZ 3** as a yellow solid. (Yield: 240 mg, 65%). ¹**H NMR** (400 MHz, CDCl₃): δ 7.45 (s, 4H), 7.31-7.28 (m, 4H), 7.17-7.11 (m, 4H), 6.92 (t, J = 8 Hz, 2H), 6.85 (d, J = 8 Hz, 2H), 6.79 (d, J = 8 Hz, 2H), 3.81 (t, J = 8 Hz, 4H), 1.88-1.79 (m, 4H), 1.01 (t, J = 4 Hz, 6H); ¹³C NMR (100 MHz, CDCl₃): δ 145.46, 144.56, 131.31, 130.77, 130.15, 127.46, 127.31, 124.81, 124.16, 122.98, 122.72, 116.73, 115.53, 115.02, 90.74, 89.04, 49.28, 20.07, 11.26 ppm; **HRMS (ESI, positive)**: m/z [M]⁺ calculated for C40H32N2S2 604.2007, found 604.2001.

Compound 4: In 100mL round bottomed flask, ethynyl-PTZ (100 mg,0.37 mmol) and iodobenzene (76 mg (0.041 mL), 0.37 mmol) were dissolved in THF: Triethylamine (4:1, v/v; 50 mL), and reaction mixture was purged with argon, and Pd(PPh₃)₄ (21 mg, 0.01 mmol), and CuI (3.5 mg, 0.01mmol) were added. The reaction mixture was stirred at 60 °C for 12 h. Upon the completion of the reaction, the solvent was evaporated and purified by silica gel column chromatography with hexane to get the desired compound **4** as yellow solid. (Yield: 80 mg, 62%). ¹**H NMR (400 MHz, DMSO-d₆):** δ 7.51-7.50 (m, 2H), 7.41-7.34 (m, 4H), 7.30 (s, 1H), 7.20 (t, J = 4 Hz, 1H), 7.14 (d, J = 8 Hz, 1H), 7.03-7.00 (m, 2H), 6.96 (t, J = 8 Hz, 1H), 3.84 (t, J = 8 Hz, 2H), 1.73-1.65 (m, 2H), 0.93 (t, J = 8 Hz, 3H); ¹³**C NMR (100 MHz, CDCl₃):** δ 145.38, 144.72, 143.90, 131.53, 131.04, 130.81, 130.29, 130.23, 130.05, 129.73, 128.39, 128.09, 127.54, 127.38,

124.88, 124.28, 123.53, 122.78, 117.47, 117.05, 116.74, 115.60, 115.11, 89.24, 88.97, 49.34, 20.16, 11.36 ppm; **HRMS (ESI, positive):** m/z [M+ nH]⁺ calculated for C23H19NS 342.1311, found 342.1344.

Compound 1a: In a 100 mL round bottomed flask, tetracyanoethylene (TCNE, 72 mg, 0.56 mmol) was added to solution of compound 1 (150 mg, 0.28 mmol) in DCM (50 mL). The reaction mixture was heated at 40 °C for 4 h. After completion of reaction, the reaction mix. was dried under vacuum and purified by column chromatography with hexane/DCM (1:4, v/v) as eluent to give 1a as dark purple black solid (Yield: 160 mg, 86%). ¹H NMR (400 MHz, CDCl₃): δ 7.68-7.65 (m, 1H), 7.43-7.39 (m, 2H), 7.28 (d, J = 1.76 Hz, 1H), 7.19-7.14 (m, 2H), 7.07 (d, J = 8 Hz, 2H), 7.01-6.95 (m, 2H), 6.89-6.86 (m, 3H), 6.80 (d, J = 8 Hz, 1H), 3.88-3.82 (m, 4H), 1.90-1.78 (m, 4H), 1.06-1.00 (m, 6H). ¹³C NMR (100 MHz, CDCl₃): δ 160.72, 151.16, 149.69, 148.44, 142.86, 142.04, 134.21, 131.70, 130.38, 129.78, 127.88, 127.63, 127.53, 125.46, 125.11,124.41, 123.92, 123.21, 122.67, 120.75, 116.18, 116.09, 115.10, 114.96, 112.80, 112.11, 111.94, 111.70, 110.63, 91.37, 88.19, 80.57, 49.95, 20.01, 11.11 ppm; HRMS (ESI, positive) m/z [M + Na] + calculated for C40H28N6S2 679.1708, found 679.1709.

Compound 1b: In 100 mL round bottomed flask, tetracyanoquinodimethane (TCNQ, 154 mg, 0.75 mmol) was added in solution of compound **1** (200 mg, 0.37 mmol) in DCE (50 mL) under argon atmosphere. The reaction mixture was heated at 80 °C overnight. After the completion of reaction, the solvent was removed under vacuum and product was purified by column chromatography with hexane /DCM (1:4, v/v) as eluent to yield **1b** as dark brown solid (Yield: 210 mg, 75%). **1H NMR (400 MHz, CDCl₃):** δ 8.12 (s, 2H), 7.20-7.16 (m, 3H), 7.09 (d, J = 3.9 Hz, 2H), 7.00-6.95 (m, 5H), 6.92-6.88 (m, 6H), 3.87 (t, J = 8 Hz, 4H), 1.89-1.82 (m, 4H), 1.05-1.02 (m, 6H); **13C NMR (100 MHz, CDCl₃):** δ 153.57, 152.63, 148.54, 144.79, 143.47, 137.88, 131.20, 129.37, 127.79, 127.53, 126.37, 123.64, 123.13, 116.01, 115.56, 113.90, 113.25, 110.25, 91.84, 80.50, 49.80, 19.98, 11.20 ppm; **HRMS (ESI, positive)** m/z [M + nH] + calculated for C46H32N6S2 733.2203, found 733.2238.

Compound 2a: In 100 mL round bottomed flask, tetracyanoethylene (TCNE, 83 mg, 0.65 mmol) was added to a solution of compound **2** (150 mg, 0.29 mmol) in CH₂Cl₂ (50 mL), and the mixture was stirred at 40 °C for 4 h. After the reaction was complete, the solvent was removed in vacuum and the product was purified by column chromatography hexane/DCM (1:4, v/v) (eluent: CH₂Cl₂)

to give **2a** as a dark-violet solid (yield: 160 mg, 85 %). ¹H NMR (**400** MHz, CDCl₃): δ 7.68-7.65 (m, 1H), 7.43-7.39 (m, 2H), 7.28 (d, J = 3.9 Hz, 1H), 7.19-7.14 (m, 2H), 7.08 (d, J = 8 Hz, 2H), 7.01-6.95 (m, 2H), 6.89-6.86 (m, 3H), 6.80 (d, J = 8 Hz, 1H), 3.88-3.82 (m, 4H), 1.89-1.78 (m, 4H), 1.06-1.00 (m, 6H); ¹³C NMR (**100** MHz, CDCl₃): δ 160.75, 151.19, 149.72, 148.47, 142.89, 142.07, 134.23, 131.73, 130.41, 127.91, 127.70, 127.66, 127.58, 125.49, 125.14, 124.44, 123.95, 123.25, 122.70, 120.77, 116.21, 116.12, 115.12, 114.99, 112.83, 112.13, 111.97, 111.73, 110.65, 91.41, 88.22, 80.61, 49.98, 20.04, 11.14 ppm; MALDI-TOF m/z [M]⁺ calculated for C38H28N6S2 632.1817, found 632.075.

Compound 2b: In 100 mL round bottomed flask, tetracyanoquinodimethane (TCNQ, 97 mg, 0.47 mmol) was added to solution of compound **2** (200 mg, 0.39 mmol) in DCE (50 mL) under argon atmosphere. The reaction mixture was heated at 80 °C for overnight. After completion of reaction, the reaction mixture was dried under reduced pressure and purified by column chromatography with hexane/DCM (1:4, v/v) (eluent: CH₂Cl₂) to get **2b** as dark brown black solid (Yield: 120 mg, 75%). ¹**H NMR (400 MHz, CDCl₃):** δ 7.55 (d, *J* = 8 Hz, 3H), 7.47 (d, *J* = 12 Hz, 2H), 7.33 (d, *J* = 4 Hz, 1H), 7.19-7.13 (m, 4H), 7.09-7.04 (m, 2H), 6.99-6.94 (m, 3H), 6.87-6.79 (m, 3H), 3.85-3.80 (m, 4H), 1.87-1.80 (m, 4H), 1.05-1.00 (m, 6H); ¹³**C NMR (100 MHz, CDCl₃):** δ 168.11, 154.04, 150.48, 149.57, 148.69, 142.82, 142.20, 134.72, 134.14, 133.18, 131.85, 129.23, 128.12, 127.85, 127.77, 127.58, 127.04, 126.15, 126.01, 125.58, 125.28, 124.22, 123.84, 122.97, 122.72, 116.09, 115.98, 115.30, 114.98, 113.78, 113.59, 113.06, 81.75, 75.60, 49.82, 49.72, 20.05, 19.98, 11.19, 11.12 ppm; **HRMS (ESI, positive)** m/z [M + Na] + calculated for C44H32N6S2 731.2026, found 731.2022.

Compound 3a: In 100mL round bottomed flask, tetracyanoethylene (TCNE, 46.6 mg, 0.36 mmol) was added to a solution of compound 3 (100 mg, 0.16 mmol) in CH₂Cl₂ (50 mL), and the mixture was stirred at 40 °C for 6 h. After the reaction was complete, the solvent was removed under vacuum and the product was purified by using column chromatography with hexane/DCM (1:4, v/v) (eluent: CH₂Cl₂) to give 3a as a dark-violet solid (Yield: 98 mg, 80%). ¹H NMR (400 MHz, CDCl₃): δ 7.70-7.59 (m, 5H), 7.38-7.28 (m, 3H), 7.23-7.06 (m, 4H), 7.02-6.86 (m, 5H), 6.80 (d, J = 8 Hz, 1H), 3.88-3.81 (m, 4H), 1.88-1.80 (m, 4H), 1.06-1.00 (m, 6H); ¹³C NMR (100 MHz, CDCl₃): δ 166.41, 163.36, 151.35, 146.41, 144.28, 141.86, 132.52, 131.34, 130.66, 130.47, 130.02, 129.44, 127.98, 127.71, 127.58, 127.51, 127.44, 125.71, 125.00, 124.61, 124.26, 123.96,

123.01, 122.58, 116.25, 115.68, 115.55, 115.09, 112.79, 112.11, 111.89, 111.33, 108.18, 95.82, 88.36, 86.43, 80.73, 49.37, 20.03, 11.13 ppm; **HRMS (ESI, positive)** m/z [M] ⁺ calculated for C46H32N6S2 732.2128, found 732.2124.

Compound 3b: In 100 mL round bottomed flask, tetracyanoquinodimethane (TCNQ, 74 mg, 0.36 mmol) was added to solution of compound 3 (100 mg, 0.16 mmol) in DCE (50 mL) under argon atmosphere. The reaction mixture was heated at 80 °C for overnight. After completion of reaction, the reaction mixture was dried under vacuum and purified by column chromatography with hexane/DCM (1:4, v/v) (eluent: CH₂Cl₂) 3b as dark purple black solid (Yield: 102 mg, 76%). ¹H NMR (400 MHz, CDCl₃): δ 7.62-7.53 (m, 6H), 7.47-7.44 (m, 2H), 7.32-7.29 (m, 2H), 7.18-7.13 (m, 2H), 7.11-7.07 (m, 2H), 7.04-6.91 (m, 4H), 6.87-6.77 (m, 4H), 3.84-3.79 (m, 4H), 1.86-1.77 (m, 4H), 1.04-0.99 (m, 6H); ¹³C NMR (100 MHz, CDCl₃): δ 170.07, 153.82, 148.76, 146.29, 144.29, 142.79, 134.76, 133.84, 132.38, 131.73, 131.44, 131.22, 130.44, 130.38, 129.71, 129.61, 129.33, 128.77, 127.82, 127.63, 127.49, 127.45, 126.50, 126.42, 125.73, 124.96, 123.92, 123.92, 122.99, 116.82, 116.04, 115.88, 115.62, 115.29, 115.07, 113.71, 113.64, 112.73, 112.35, 95.02, 88.30, 86.58, 49.75, 20.06, 11.20 ppm; HRMS (ESI, positive) m/z [M] + calculated for C52H36N6S2 808.2437, found 808.2435.

Compound 4a: In a 100 mL round bottomed flask, tetracyanoethylene (TCNE, 37 mg, 0.29 mmol) was added to solution of compound 4 (100 mg, 0.29 mmol) in DCM (50 mL). The reaction mixture was heated at 40 °C for 4 h. After completion of reaction, the reaction mix. was dried under vacuum and purified by column chromatography with hexane/DCM (30:70, v/v) as eluent to give 4a as dark purple black solid (Yield: 110 mg, 80%). ¹H NMR (400 MHz, CDCl₃): δ 7.70 (t, J = 12 Hz, 4H), 7.57 (t, J = 8 Hz, 2H), 7.39 (s, 1H), 7.19 (t, J = 8 Hz, 1H), 7.08 (d, J = 8 Hz, 1H), 7.02 (t, J = 8 Hz, 1H), 6.89 (t, J = 8 Hz, 2H), 3.87 (t, J = 8 Hz, 2H), 1.93-1.80 (m, 2H), 1.06 (t, J = 8 Hz, 3H); ¹³C NMR (100 MHz, CDCl₃): δ 167.76, 163.43, 151.28, 141.83, 134.57, 131.33, 130.43, 129.97, 129.34, 127.96, 127.65, 127.56, 125.65, 124.57, 124.12, 122.53, 116.23, 115.07, 112.73, 112.09, 111.68, 111.12, 87.50, 80.65, 49.97, 19.99, 11.09 ppm; HRMS (ESI, positive) m/z [M + Na] + calculated for C29H19N5S 492.1253, found 492.1247.

Compound 4b: In 100 mL round bottomed flask, tetracyanoquinodimethane (TCNQ, 59 mg, 0.29 mmol) was added in solution of compound 4 (100 mg, 0.29 mmol) in DCE (50 mL) under argon atmosphere. The reaction mixture was heated at 80 °C for 12 h. After the completion of reaction,

the solvent was removed under vacuum and product was purified by column chromatography with hexane /DCM (20:80, v/v) as eluent to yield compound **4b** as dark greenish colored solid (Yield: 120 mg, 75%). ¹**H NMR (400 MHz, CDCl₃):** δ 7.64-7.56 (m, 3H), 7.52-7.45 (m, 3H), 7.31 (d, J = 8 Hz, 1H), 7.24 (s, 1H), 7.18 (t, J = 8 Hz, 1H), 7.13-7.08 (m, 2H), 7.05-6.96 (m, 3H), 6.88-6.82 (m, 2H), 3.83 (t, J = 8 Hz, 2H), 1.89-1.80 (m, 2H), 1.03 (t, J = 8 Hz, 3H); ¹³**C NMR (100 MHz, CDCl₃):** δ 171.44, 153.90, 149.03, 148.77, 142.87, 134.86, 133.94, 133.86, 133.71, 133.78, 129.86, 129.54, 129.40, 128.78, 127.89, 127.66, 126.48, 126.39, 125.73, 123.96, 122.98, 116.09, 115.34, 113.76, 113.72, 112.68, 112.27, 87.39, 49.79, 20.10, 11.25 ppm; **HRMS (ESI, positive)** m/z [M + nH] + calculated for C35H23N5S 546.1747, found 546.1750.

Supporting Information

Experimental and synthetic details, ¹H and ¹³C NMR, HRMS, and MALDI-mass of synthesized compounds. Additional CVs, spectroelectrochemical, and fs-TA spectral data. Coordinates of optimized geometries.

Acknowledgments

This research was supported by the US-National Science Foundation (2000988 to FD), Council of Scientific and Industrial Research (Project No. CSIR 01(2934)/18/EMR-II), New Delhi, and SERB (Project No. CRG/2018/000032) New Delhi, Govt. of India. We gratefully acknowledge the Sophisticated Instrumentation Centre (SIC), IIT Indore. IY is thankful to CSIR, India for a research fellowship.

Conflict of Interest

There are no conflicts to declare.

Data Availability Statement

The data that support the findings of this study are available from the corresponding author upon reasonable request.

Keywords: push-pull phenothiazines, excited-state charge separation, spectroelectrochemistry, cyclic voltammetry, pump-probe transient spectroscopy.

- 1. M. Kaltenbrunner, M. S. White, E. D. Głowacki, T. Sekitani, T. Someya, N. S. Sariciftci, S. Bauer, *Nat. Commun.* **2012**, *3*, 770.
- 2. C. J. Brabec, M. Heeney, I. McCulloch, J. Nelson, Chem. Soc. Rev. 2011, 40, 1185–1199.
- 3. Y. Cui, H. Yao, J. Zhang, T. Zhang, Y. Wang, L. Hong, K. Xian, B. Xu, S. Zhang, J. Peng, Z. Wei, F. Gao, J. Hou, *Nat. Commun.* **2019**, *10*, 2515.
- 4. S. D. Collins, N. A. Ran, M. C. Heiber, T.-Q. Nguyen, *Adv. Energy Mater.* **2017**, *7*, 1602242.
- 5. Y. Chen, X. Wan, G. Long, Acc. Chem. Res. 2013, 46, 2645–2655.
- 6. Z. Wu, Y. Liu, L. Yu, C. Zhao, D. Yang, X. Qiao, J. Chen, C. Yang, H. Kleemann, K. Leo, D. Ma, *Nat. Commun.* **2019**, *10*, 2380. DOI:10.1038/s41467-019-10104-4.
- 7. J. Kido, M. Kimura, K. Nagai, Science 1995, 267, 1332–1334.
- 8. C. Yang, X. Wang, Z. Xu, M. Wang, Sens. Actuators B Chem. 2017, 245, 845–852.
- 9. G. N. M. van der Krogtl, J. Oginkl, B. Ponsioen, K. Jalink, *PLoS ONE* **2008**, *3*, e1916.
- 10. C. Fan1, K. W. Plaxco, A. J. Heeger, *Trends Biotechnol.* **2005**, *23*, 186-192.
- 11. Y. Li, J.-Y. Liu, Y.-D. Zhao, Y.-C. Cao, Mater. Today 2017, 20, 258-266.
- 12. Y. Wang, Y. Duan, R. Guo, S. Ye, K. Di, W. Zhang, S. Zhuang, L. Wang, *Org. Electron.* **2021**, *97*, 106275.
- 13. J. Zhang, J. Jin, H. Xu, Q. Zhang, W. Huang, J. Mater. Chem. C, 2018, 6, 3485-3498.
- 14. B. Basheer, D. Mathew, B. K. George, C. R. Nair, Sol. Energy 2014, 108, 479–507.
- 15. H. Tian, X. Yang, R. Chen, Y. Pan, L. Li, A. Hagfeldt, L. Sun, *Chem. Commun.*, **2007**, 3741–3743.
- 16. Z.-S. Huang, H. Meier, D. Cao, J. Mater. Chem. C 2016, 4, 240-2426.
- 17. A. S. Hart, C. B. KC, N. K. Subbaiyan, P. A. Karr, F. D'Souza, *ACS Appl. Mater. Interfaces* **2012**, *4*, 5813–5820.
- 18. T. Michinobu, F. Diederich, *Angew. Chem. Int. Ed.* **2018**, *130*, 3612–3638.
- 19. A. T. Bui, C. Philippe, M. Beau, N. Richy, M. Cordier, T. Roisnel, L. Lemie gre, O. Mongin, F. Paul, Y. Trolez, *Chem. Commun.* **2020**, *56*, 3571–3574.
- 20. Z. Pokladek, N. Ripoche, M. Betou, Y. Trolez, O. Mongin, J. O. Banska, K. Matczyszyn, M. Samoc, M. G. Humphrey, M. B. Desce, F. Paul, *Chem. Eur. J.* **2016**, *22*, 1-14.
- a) T. Shoji, S. Ito, *Chem. Eur. J.* 2017, 23, 16696-16709. b) P. S. Marques, J. M. A. Castan, B. A. L. Raul, G. Londi, I. Ramirez, M. S. Pshenichnikov, D. Beljonne, K. Walzer, M. Blais, M. Allain, C. Cabanestos, P. Blanchard, *Chem. Eur. J.* 2020, 26, 16422-16433.
- 22. P. Gautam, R. Sharma, R. Misra, M. L. Keshtov, S. A. Kuklin, G. D. Sharma, *Chem. Sci.* **2017**, *8*, 2017-2024.
- 23. Y. Patil, R. Misra, R. Singhal, G. D. Sharma, J. Mater. Chem. A 2017, 5, 13625-13633.
- M. Sekita, B. Ballesteros, F. Diederich, D. M. Guldi, G. Bottari, T. Torres, *Angew. Chem. Int. Ed.* 2016, 55, 5560-5564.
- 25. K. A. Winterfeld, G. Lavarda, J. Guilleme, M. Sekita, D. M. Guldi, T. Torres, G. Bottari, *J. Am. Chem. Soc.* **2017**, *139*, 5520-5529.

- a) K. A. Winterfeld, G. Lavarda, J. Guilleme, D. M. Guldi, T. Torres, G. Bottari, *Chem. Sci.* 2019, 10, 10997-11005; b) L. M. Mateo, L. Sagresti, Y. Luo, D. M. Guldi, T. Torres, G. Brancato, G. Bottari, *Chem. Eur. J.* 2021, 27, 16049-16055.
- a) F. Tancini, F. Monti, K. Howes, A. Belbakra, A. Listorti, W. B. Schweizer, P. Reutenauer, J.L. Alonso-Gomez, C. Chiorboli, L. M. Urner, J.-P. Gisselbrecht, C. Boudon, N. Armaroli, F. Diederich, *Chem. Eur. J.* 2014, 20, 202-216; b) H. Gotfredsen, T. Neumann, F. E. Storm, A. V. Muñoz, M. Jevric, O. Hammerich, K. V. Mikkelsen, M. Freitag, G. Boschloo, M. B. Nielsen, *ChemPhotoChem* 2018, 2, 976-985.
- 28. T. Shoji, S. Ito, K. Toyota, M. Yasunami, N. Morita, *Chem. Eur. J.* **2008**, *14*, 8398-8408.
- 29. A. Gopinath, N. Manivannan, S. Mandal, N. Mathivanan, A. S. Nasar, *J. Mater. Chem. B* **2019**, *7*, 6010-6023.
- 30. T. Michinobu, Chem. Soc. Rev. 2011, 40, 2306-2316.
- a) A. T. Bui, C. Philippe, M. Beau, N. Richy, M. Cordier, T. Roisnel, L. Lemiegre, O. Mongin, F. Paul, Y. Trolez, *Chem. Commun.* 2020, 56, 3571-3574. b) H. Gotfredsen, T. Neumann, F. E. Storm, A. V. Munoz, M. Jevric, O. Hammerich, K. V. Mikkelsen, M. Freitage, G. Boschloo, M. B. Nielsen, *ChemPhotoChem* 2018, 2, 976-985.
- 32. P. Gautam, R. Misra, M. B. Thomas, F. D'Souza, Chem. Eur. J. 2017, 23, 9192-9200.
- 33. R. Sharma, M. B. Thomas, R. Misra, F. D'Souza, *Angew. Chem. Int. Ed.* **2019**, *58*, 4350-4355.
- 34. Y. Rout, Y. Jang, H. B. Gobeze, R. Misra, F. D'Souza, *J. Phys. Chem. C* **2019**, *123*, 23382-23389.
- 35. M. Poddar, Y. Jang, R. Misra, F. D'Souza, Chem. Eur. J. 2020, 26, 6869-6878.
- 36. D. Pinjari, A. Z. Alsaleh, Y. Patil, R. Misra, F. D'Souza, *Angew. Chem. Int. Ed.* **2020**, *59*, 23697-23705.
- 37. I. S. Yadav, A. Z. Alsaleh, R. Misra, F. D'Souza, Chem. Sci. 2020, 12, 1109-1120.
- a) Y. Jang, Y. Rout, R. Misra, F. D'Souza, J. Phys. Chem. B 2021, 125, 4067-4075; b) F. Khan, Y. Jang, Y. Patil, R. Misra, F. D'Souza, Angew. Chem. Int. Ed. 2021, 60, 20518-20527; c) J. Sinde, M. B. Thomas, M. Poddar, R. Misra, F. D'Souza, J. Phys. Chem. C 2021, 125, 23911-23921. d) B. Sekaran, A. Dawson, Y. Jang, K. V. MohanSingh, R. Misra, F. D'Souza, Chem. Eur. J. 2021, 27, 14335-14344.
- 39. T. J. J. Müller, Tetrahedron 1999, 40, 6563-6566.
- 40. C. S. Krämer, T. J. J. Müller, Eur. J. Org. Chem. **2003**, 3534-3548.
- 41. Gaussian 09, Revision C.01, M. J. Frisch, G. W. Trucks, H. B. Schlegel, G. E. Scuseria, M. A. Robb, J. R. Cheeseman, G. Scalmani, V. Barone, B. Mennucci, G. A. Petersson, H. Nakatsuji, M. Caricato, X. Li, H. P. Hratchian, A. F. Izmaylov, J. Bloino, G. Zheng, J. L. Sonnenberg, M. Hada, M. Ehara, K. Toyota, R. Fukuda, J. Hasegawa, M. Ishida, T. Nakajima, Y. Honda, O. Kitao, H. Nakai, T. Vreven, J. A., Jr., Montgomery, J. E. Peralta, F. Ogliaro, M. Bearpark, J. J. Heyd, E. Brothers, K. N. Kudin, V. N. Staroverov, R. Kobayashi, J. Normand, K. Raghavachari, A. Rendell, J. C. Burant, S. S. Iyengar, J. Tomasi,

- M. Cossi, N. Rega, J. M. Millam, M. Klene, J. E. Knox, J. B. Cross, V. Bakken, C. Adamo, J. Jaramillo, R. Gomperts, R. E. Stratmann, O. Yazyev, A. J. Austin, R. Cammi, C. Pomelli, J. W. Ochterski, R. L. Martin, K. Morokuma, V. G. Zakrzewski, G. A. Voth, P. Salvador, J. J. Dannenberg, S. Dapprich, A. D. Daniels, Ö. Farkas, J. B. Foresman, J. V. Ortiz, J. Cioslowski, D. J. Fox, Gaussian, Inc., Wallingford, CT, USA, **2009**.
- 42. D. Rehm, A. Weller, *Isr. J. Chem.*, **1970**, *8*, 259-271.
- 43. Gibbs free-energy change associated with excited-state charge separation (CS) and dark charge recombination (CR) were estimated according to equations i-iii

$$-\Delta G_{\rm CR} = E_{\rm ox} - E_{\rm red} + \Delta G_{\rm S} \tag{i}$$

$$-\Delta G_{\rm CS} = \Delta E_{00} - (-\Delta G_{\rm CR})$$
 (ii)

where ΔE_{00} corresponds to the singlet state energy of 1. The term $\Delta G_{\rm S}$ refers to electrostatic energy calculated according to dielectric continuum model (see equation iii). The $E_{\rm ox}$ and $E_{\rm red}$ represent the oxidation potential and the first reduction potential, respectively.

$$\Delta G_{\rm S} = e^2/4 \pi \, \varepsilon_{\rm o} \, (-1/R_{\rm cc} \, \varepsilon_{\rm R})$$
 (iii)

The symbols ε_0 and ε_R represent the vacuum permittivity and dielectric constant of benzonitrile used for photochemical and electrochemical studies. R_{CC} is the center-to-center distance between donor and acceptor entities from the computed structures.

44. J. Snellenburg, S. Laptenok, R. Seger, K. Mullen, I. van Stokkum, *J. Stat. Softw.* **2012**, *49* 1-22.

Table of content

Near-IR Intramolecular Charge Transfer in Strongly Interacting Diphenothiazene-TCBD and Diphenothiazene-DCNQ Push-Pull Triads

I. S. Yadav, Y. Jang, Y. Rout, M. B. Thomas, R. Misra* and F. D'Souza*

